ATLAS NOTE

ATLAS-CONF-2011-065

April 20, 2011

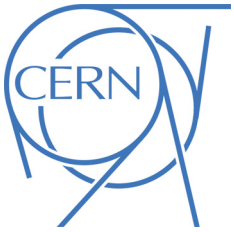

Search for strong gravity effects in same-sign dimuon final states

The ATLAS Collaboration

Abstract

A search for mini black holes has been performed in a same sign dimuon final state using 31 pb^{-1} of proton-proton collision data collected by the ATLAS detector at a centre of mass energy of 7 TeV at the CERN Large Hadron Collider. Using the total number of charged particles to define the signal region, the data are found to be consistent with the expectation from the Standard Model. These results are used to set upper limits on the cross section for new physics to this final state. Exclusion contours are derived in the context of a low scale gravity model.

1 Introduction

Models introducing extra dimensions can provide a solution to the hierarchy problem in which the Planck scale $M_{\mathrm{Pl}} \sim 10^{15}$ TeV is much larger than the electroweak scale. In some models of extra dimensions, the gravitational field can propagate into (n+4)-dimensions, where n is the number of extra dimensions, while the Standard Model particles are restricted to four dimensional space-time. Therefore, the gravitational field as measured in four dimensions is reduced in strength from the fundamental gravitational field. As a result, the fundamental Planck scale in $(n+4)$-dimensions M_{D} would be much smaller than the Planck scale in four dimensions M_{Pl}, and possibly comparable to the electroweak scale.

One model of extra dimensions is the ADD model, which is a model of large flat extra dimensions, proposed by Arkani-Hamed, Dimopoulos, and Dvali [1, 2, 3]. The experimental lower limits on the value of M_{D} in this model from collider experiments are $M_D > 1.60, 1.20, 1.04, 0.98, 0.94, 0.80$ TeV for n =2, 3, 4, 5, 6, and 7, respectively [4, 5, 6].

If extra dimensions exist and M_{D} is in the TeV range, microscopic black holes with TeV scale mass can exist and they could be produced by the Large Hadron Collider. Black holes are thought to be produced when half the classical impact parameter of two colliding partons is less than the higher-dimensional horizon radius corresponding to a black hole with mass m equal to the invariant mass of the colliding parton system [7, 8]. This paper considers higher-dimensional Schwarzschild solutions, as well as Kerr solutions for black holes with initial angular momentum equal to the relative angular momentum between the two colliding partons; parton spin is ignored. The decay of a black hole is expected to have the characteristics of Hawking radiation [9].

The production of black holes in a proton-proton collider occurs with a continuous mass distribution ranging from approximately the reduced Planck scale M_{D} to the proton-proton centre of mass energy of 7 TeV. The classical approximations used for black hole production and the semi-classical approximations for its decay are only valid for masses well above the Planck scale. A lower threshold M_{TH} is thus applied to the black hole mass to reduce the contributions from regions where the models are invalid. The production cross section is set to zero if the parton-parton center of mass energy is below M_{TH}.

Once produced, a black hole evaporates initially by Hawking radiation. The black hole emits all particles kinematically allowed including quarks, gluons, leptons, W-bosons, where the relative fractions are determined by the number of degrees of freedom of each particle and the emissivity for the decay of each type of particle. Black hole events should therefore have a high multiplicity of high-p_{T} particles which is the characteristic feature exploited in this analysis. No graviton initial-state radiation or emission from the black hole is considered in this paper. As a result of the emission of Hawking radiation, the mass of the produced black hole declines. When the mass of the black hole approachesM_{D}, quantum gravity effects become important, but these are not considered in this paper. In the final stage of the black hole decay, the classical evaporation is no longer a good description. In such cases where the black hole mass is near the Planck scale, the burst model adopted by the BlackMax event generator [10, 11] is used to model the final part of the decay.

A search for mini blackholes in a multijet final state is presented in Ref. [12, 13]. In this complementary analysis, a final state with two muons of the same charge is considered since the Standard Model has low rates of production to this final state. Muons can be produced directly from the black hole; these muons have very little activity around them in the detector (*isolated* muons). On the other hand, muons which are produced in cascade decays of the black hole to t-quark, and from the semi-leptonic decay of b, c quarks can have several other tracks close by (non-isolated muons). In order to maintain good acceptance for a possible signal, only one of the muons is required to be isolated in this analysis.

The decay of the black hole to multiple high p_{T} objects is used to divide the observed events into background rich and potentially signal rich regions. This is done by using the total number of charged tracks as the criterion to assign events to each region. Black hole events typically have a high number

of tracks per event, while Standard Model processes have sharply falling track multiplicity distributions. After this event selection, the number of events in data are compared to the background prediction.

The backgrounds from Standard Model processes are divided into two categories; processes that produce same-sign dimuons in distinct decay trees and processes where the two muons come from connected decay trees following the characterization in Ref. [14]. Dimuon events in distinct decay trees arise predominantly from the W+jets process, where the leading isolated muon comes from W-boson decay and the other muon comes from a π/K decay-in-flight, or the semi-leptonic decay of a b or c hadron. This background also has contributions from the Z+jets process, and low p_{T} QCD. The background from distinct decay trees is the largest background and is estimated completely from data.

Dimuon events in connected decay trees are produced in the decays of $t\bar{t}$ events and $b\bar{b}$ events. In $t\bar{t}$ events, the most likely case is that the leading isolated muon arises from the decay of a W-boson from one of the top-quarks, and the other muon of same charge comes from the semileptonic decay of a b-quark from the other top-quark. In $b\bar{b}$ events, the leading muon arises from the semileptonic decay of one b-quark; the other muon comes from the sequential decay $b \to cX \to \mu X'$. Same-sign dimuons can also be produced due to $B^0\bar{B}^0$ mixing. The backgrounds from $t\bar{t}$ and $b\bar{b}$ are estimated from MC samples.

2 Experimental Setup

The ATLAS detector [15] covers nearly the entire solid angle [1] around the collision point with layers of tracking detectors, calorimeters and muon chambers. The inner detector (ID) is immersed in a 2 T magnetic field along z-axis and provides charged particle tracking in the range $|\eta| < 2.5$. The silicon pixel detector covers the vertex region and typically provides three measurements per track, followed by the silicon microstrip tracker (SCT) which provides four measurements from eight strip layers. The silicon detectors are complemented by the transition radiation tracker (TRT) which provides more than 30 straw-tube measurements per track and improves the inner detector momentum resolution.

The calorimeter system covers the pseudorapidity range $|\eta| < 4.9$. Lead-liquid argon (LAr) electromagnetic sampling calorimeters cover the range $|\eta| < 3.2$, with an additional thin LAr presampler covering $|\eta| < 1.8$ to correct for energy loss in material upstream of the calorimeters. Hadronic calorimetry is provided by a scintillator-tile calorimeter within $|\eta| < 1.7$ and two copper/LAr endcap calorimeters. The solid angle coverage is completed with forward copper/LAr and tungsten/LAr calorimeters for electromagnetic and hadronic measurements respectively.

The muon spectrometer comprises of separate trigger and high-precision tracking chambers which measure the deflection of muon tracks in a magnetic field with a bending integral of approximately 2 to 8 Tm in the central region. The magnetic field is generated by three superconducting air-core toroids. The chamber system covers the region $|\eta| < 2.7$ with three layers of monitored drift tubes. The muon trigger system covers the range $|\eta| < 2.4$ with resistive plate chambers in the barrel, and thin gap chambers in the endcap regions.

3 Data and Monte Carlo samples

The data used in this analysis were collected in 2010 with the LHC operating at a centre of mass energy of 7 TeV. The total integrated luminosity after stable beam, and basic detector and data-quality requirements is 31 pb^{-1}, with an uncertainty of 3.4% [16]. The data were collected with a single muon trigger

[1] ATLAS uses a right-handed coordinate system with its origin at the nominal interaction point (IP) in the centre of the detector and the z-axis coinciding with the axis of the beam pipe. The x-axis points from the IP to the centre of the LHC ring, and the y-axis points upward. Cylindrical coordinates (r,ϕ) are used in the transverse plane, ϕ being the azimuthal angle around the beam pipe. The pseudorapidity is defined in terms of the polar angle θ as $\eta = -\ln\tan(\theta/2)$.

with threshold of 15 GeV on the muon's transverse momentum. The trigger efficiency is independent of p_{T} for the muons above 20 GeV that are used in this analysis.

Background Monte Carlo (MC) simulated samples were generated for the $t\bar{t}$ and $b\bar{b}$ processes. The $t\bar{t}$ events were generated with MC@NLO [17, 18] with an assumed top-quark mass of 172.5 GeV, and with the leading order MRST2007 [19] parton distribution function (PDF) set. Fragmentation and hadronization of the events is done with Herwig [20] using Jimmy [21] for the underlying event model. The $b\bar{b}$ MC sample used in this analysis is generated and hadronized with Pythia with the MRST2007 PDF set. It is produced with a filter at the generator level requiring two muons with $p_{\mathrm{T}} > 4$ GeV each. The $b\bar{b}$ sample is limited in statistics. A crosscheck of the $b\bar{b}$ prediction in the signal region is done by comparing the prediction with an alternate $b\bar{b} + c\bar{c}$ sample which has four and half times the integrated luminosity of the $b\bar{b}$ sample. The $b\bar{b} + c\bar{c}$ sample is generated with Pythia with the MRST2007 PDF set. It has been filtered at the generator level to have two muons with $p_{\mathrm{T}} > 10$ GeV each. This filter is close to the offline p_{T} selection for candidate muons and makes this sample unusable as the nominal sample. For each of the $t\bar{t}$ and $b\bar{b}$ samples the other parameters are as described by the ATLAS MC09 tune [22].

Signal MC samples were generated using BlackMax 2.01 and the hadronization was done with Pythia . The samples were generated with the CTEQ66 [23] and MRST2007 PDF sets with the mass of the blackhole used as the QCD scale. The two PDF sets are considered since the difference in estimates from either one is outside the range of errors on each. For the signal samples, M_D was varied between 0.5 TeV and 2 TeV, M_{TH} was varied between 2 TeV and 5 TeV. In each case, samples were generated with 2, 4 and 6 extra dimensions.

4 Event Selection

Events passing the trigger are required to have at least one vertex reconstructed offline with at least five tracks. Events are discarded if a jet[2] associated with out-of-time activity or calorimeter noise is present.

Muon candidates are reconstructed from tracks measured in the muon spectrometer (MS). The MS tracks are then matched with tracks found in the inner detector (ID) using a procedure that takes material effects into account. The parameters for the resulting matched muon candidates are obtained by a statistical combination of the measurements in the MS and the ID. Requirements are made to ensure that the muon candidates point back to the primary vertex in the event, and the ratio of momenta measured in the MS and the ID is used to reduce the background from π/K decay-in-flight. The muon candidates are required to have $|\eta| < 2.4$ and the inner detector track associated to the muon is required to have sufficient hits in the pixel, SCT and TRT detectors to ensure a good measurement. At least two muon candidates passing these selections are required in each event. The muon with the highest transverse momentum is required to have $p_{\mathrm{T}} > 20$ GeV. This leading muon is also required to be isolated by requiring that the sum of transverse momenta of tracks in a cone in $\eta - \phi$ space of radius 0.2 around the muon is less than 1.8 GeV. The muon with the next highest transverse momentum is required to have $p_{\mathrm{T}} > 10$ GeV and have the same charge as the leading muon.

The track multiplicity is constructed by counting the number of tracks with $p_{\mathrm{T}} > 8$ GeV in the inner detector. These tracks are required to have $|\eta| < 2.4$, to have the same hit requirements as the muons, and to point back to the primary vertex. By definition, the track count will include the two muon candidates. The signal region is defined by selecting events with at least ten tracks, while events with less than ten tracks are used to validate the background estimates.

All selections except the trigger and bad jet veto are made in MC events. To account for the trigger efficiency, the MC events are weighted with the efficiency measured in data, while the differences in muon

[2]Jets are reconstructed from clusters of calorimeter cells using the anti-k_t jet clustering algorithm [24] with a size parameter $R = 0.4$. Jets are corrected for calorimeter non-compensation, and other effects using p_{T} and η dependent calibration factors [25]. Only jets with $p_{\mathrm{T}} > 20$ GeV and $|\eta| < 2.5$ are considered.

reconstruction and identification are accounted for by applying p_{T} and η dependent scale factors [26, 27] to the MC events when calculating the acceptance. The tracking efficiency in data is well reproduced by the MC [28] and no scale factors are needed.

5 Background Estimation

5.1 Data based background estimate

The background from disconnected decay trees is estimated in two steps. First, the probability for a track to be reconstructed as a muon is measured in a control sample of events in data. This 'fake' probability is then applied to data events with one muon and one or more tracks to obtain a prediction for μ+fake dimuon events. The control sample consists of a selection of W-boson + track events. Events are selected with at least one isolated muon with $p_{\mathrm{T}} > 20$ GeV and missing transverse energy ($E_{\mathrm{T}}^{\mathrm{miss}}$) satisfying 20 GeV $< E_{\mathrm{T}}^{\mathrm{miss}} <$ 80 GeV. $E_{\mathrm{T}}^{\mathrm{miss}}$ is constructed from the vector sum of all calorimeter cells contained in topological clusters and is corrected for the presence of muons in the event. The transverse mass of the muon and the $E_{\mathrm{T}}^{\mathrm{miss}}$ [3] is required to be between 40 GeV and 100 GeV. These selected events are also required to have at least one track not matching the 'W-muon', with $p_{\mathrm{T}} > 10$ GeV, and of the same charge as the muon. If an event has more than one such track, then all tracks are included for the measurement. The events are also required to have fewer than ten tracks to remove the signal contribution. This forms the denominator.

For the numerator, an additional muon passing analysis selection criteria with $p_{\mathrm{T}} > 10$ GeV and of the same charge as the W-muon is required. This gives us the rate of obtaining a second muon of the same charge given a track. To avoid double-counting, the contributions to the rate from $t\bar{t}$ and $b\bar{b}$ processes are estimated from MC and subtracted from the rate. The per-track rate is measured to be $(5.8 \pm 0.9) \times 10^{-3}$. This rate is then applied to all events in data with one muon and at least one track of the same charge with $p_{\mathrm{T}} > 10$ GeV. If more than one track is found, then each track is considered in calculating a total probability for the event to be reconstructed as a dimuon event. The uncertainty on the background estimate from the nominal fake rate measurement is 13%.

To obtain an estimate of the corresponding systematic uncertainty, the fake rate is parametrized as a function of track p_{T}. The difference in background estimates from the nominal rate and the p_{T}-dependent rate gives a 65% systematic uncertainty. The fake rate is found to be independent of η. To estimate the systematic effect of the use of the W-boson control region, the rate is measured in a Z-boson control region. Events with two muons of opposite charge satisfying an invariant mass requirement ($|M_{\mu\mu} - 91.0| < 15$ GeV) are selected. In these events, the denominator is formed by requiring a track with $p_{\mathrm{T}} > 10$ GeV unmatched to the Z-muons. The numerator is formed by requiring a third muon with $p_{\mathrm{T}} > 10$ GeV. The rate thus measured in the Z-boson control region agrees with the rate measured in the W-boson control region within statistical uncertainties.

5.2 MC based background estimate

The background from $t\bar{t}$ production is obtained completely from MC simulation. The NLO production cross section of 164.6 pb [29, 30] is used to normalize the MC prediction to data. The systematic uncertainty on the $t\bar{t}$ background is evaluated following the prescription in Ref. [30]. The sources considered are choice of generator, amount of initial and final state radiation (ISR/FSR), the top-quark mass, and the uncertainties on the PDF. The largest uncertainty is 13% from the difference in $t\bar{t}$ estimate by using the CTEQ66 and the MRST2007 PDF sets. The uncertainty due to the choice of generator is evaluated

[3] The transverse mass is defined as $\sqrt{2p_{\mathrm{T}}^{\mu}p_{\mathrm{T}}^{\nu}[1 - cos(\phi^{\mu} - \phi^{\nu})]}$ where the measured $E_{\mathrm{T}}^{\mathrm{miss}}$ vector provides the neutrino information.

Source	Muon+fake (%)	$t\bar{t}$ (%)	$b\bar{b}$ (%)
Nominal fake rate	13		
p_{T} dependence of fake rate	65		
PDF		13	
ISR/FSR		10.1	
t-quark Mass		9.7	
Cross section		$^{+7}_{-9.6}$	
Generator		5.5	
Luminosity		3.4	
μ reco/trig		2.2	1.8
Nominal $b\bar{b}$ control region			5.3
Alternate $b\bar{b}$ control region			4.5
Total uncertainty	66	22	7

Table 1: Systematic uncertainties in percent on the background estimates in the signal region from various sources. μ reco/trig stands for the uncertainty due to trigger efficiency weight and muon reconstruction scale factors applied to the MC events. The other labels are explained in the text.

by comparing the predictions of MC@NLO with those of POWHEG [31] interfaced to both HERWIG or PYTHIA. The POWHEG samples are generated using the CTEQ6L1 PDF set. The uncertainty due to top-quark mass is obtained by generating $t\bar{t}$ samples with top mass ±5 GeV from the nominal choice of 172.5 GeV. The ISR/FSR uncertainty is determined by using the ACERMC generator [32] interfaced to PYTHIA, and by varying the parameters controlling ISR and FSR. There is also an additional 2.2% uncertainty on the $t\bar{t}$ estimate from trigger weight and muon reconstruction scale factors.

The background from $b\bar{b}$ production is obtained from MC samples, but the overall rate is normalized to data in a $b\bar{b}$ control region. The contribution from $c\bar{c}$ to the same-sign dimuons is expected to be much smaller than that from $b\bar{b}$. Same sign dimuon events from $c\bar{c}$ are kinematically similar to those from $b\bar{b}$ and the $b\bar{b}$ MC sample is used to model the kinematics from both $b\bar{b}$ and $c\bar{c}$ events. The $b\bar{b}$ control region is selected by requiring two muons of the same charge with $p_{\mathrm{T}} > 20, 10$ GeV respectively. The leading muon is required to be non-isolated by inverting the isolation requirement. The impact parameter (d_0) of the muon is defined as the transverse distance of closest approach of the track to the primary vertex. The impact parameter significance (d_0/d_0^{error}) for the leading muon is required to be larger than 2. The ratio of transverse momenta measured in the muon spectrometer and the inner detector for the second muon is used to remove residual π/K contamination. The $E_{\mathrm{T}}^{\mathrm{miss}}$ is required to be less than 20 GeV and events are required to have less than ten tracks. The prediction from the $b\bar{b}$ MC sample is normalized to data in this control region. The systematic uncertainty on the normalization factor is obtained by defining an alternate selection of the control region; the impact parameter signficance selection for the leading muon is changed to larger than 3 and the ratio of transverse momenta selection for the second muon is removed.

The measured normalization factor is 1.12±0.08 where the uncertainty is from combined statistical and systematic contributions. There is an additional 1.8% uncertainty on the $b\bar{b}$ estimate from the trigger weight and muon reconstruction scale factors. The shapes of the distributions of muon p_{T} and track multiplicity in the MC sample have been verified with those seen in data. The $b\bar{b}$ MC has no events left in the signal region after all selections are made. An estimate of the $b\bar{b}$ background is obtained in the following way. The $b\bar{b} + c\bar{c}$ sample, as described in Section 3, is verified to reproduce the track multiplicity distribution of the nominal $b\bar{b}$ sample. The ratio of events with more than ten tracks to events with less than ten tracks is measured in the $b\bar{b} + c\bar{c}$ sample. This ratio is then applied to the number of

Process	Events
$b\bar{b}$	154 ± 14(stat) ± 12(syst)
$t\bar{t}$	32 ± 0.3(stat) ± 8(syst) ± 1.1 (lumi)
μ+fake	146 ± 1(stat) ± 35(syst)
Predicted	332 ± 14(stat) ± 38(syst)
Observed	297

Table 2: Number of expected events from Standard Model processes and number of observed data events in the background region.

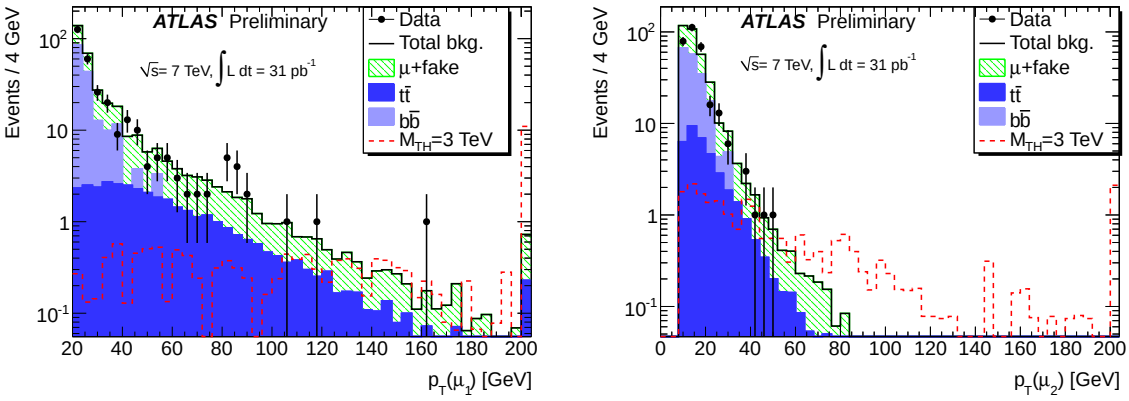

Figure 1: The leading and second muon p_{T} distributions for all same-sign dimuon events. The background histograms are stacked. The signal expectation for a non-rotating black hole model with parameters M_{D} = 630 GeV, M_{TH} = 3 TeV, and one extra dimension is overlaid for illustrative purposes. The overflows are shown in the last bin along X-axis.

events predicted by the nominal $b\bar{b}$ MC sample with less than ten tracks to obtain an estimate in the signal region (≥ ten tracks). The statistical uncertainty on the prediction is 100%.

Table 1 shows a summary of the systematic uncertainties in signal region for all the backgrounds.

The background estimation is tested in a control region. This region is defined using the same selections as the signal region, except for the track multiplicity requirement which is inverted to be less than ten tracks. The prediction from the Standard Model along with the number of observed events in data in the background region is shown in Table 2. The signal contribution in the background region has been checked to be less than one event for various choices of signal parameters. The observation agrees well with the prediction.

6 Results

Figures 1 and 2 show the p_{T} distributions for the muons and the track multiplicity in all same-sign dimuon events respectively. The prediction for a sample signal point with M_{D} = 630 GeV, M_{TH} = 3 TeV, and one extra dimension is also shown. The background predictions peak at low values of the track multiplicity whereas the signal contribution for different choices of parameters has a higher number of tracks. The signal region is defined to have at least ten tracks. The observed distributions in data agree well with the predictions from the Standard Model. Table 3 shows the expected and observed number of same-sign dimuon events in the signal region. No excess over the Standard Model predictions is observed in the

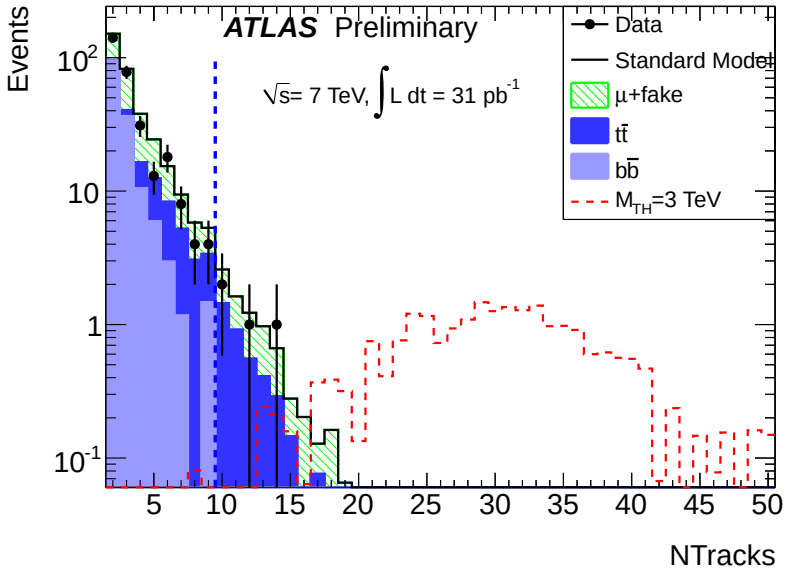

Figure 2: The track multiplicity distribution for all same-sign dimuon events. We select the region with NTracks ≥ 10 as the signal region. The background histograms are stacked. The signal expectation for a non-rotating black hole model with parameters $M_{\mathrm{D}} = 630$ GeV, $M_{\mathrm{TH}} = 3$ TeV, and one extra dimension is overlaid for illustrative purposes.

data.

Process	Events
$b\bar{b}$	0.26 ± 0.26(stat) ± 0.02(syst)
$t\bar{t}$	3.97 ± 0.10(stat) ± 0.88(syst) ± 0.13(lumi)
μ+fake	4.0± 0.3(stat) ± 2.7(syst)
Predicted	8.2 ± 0.4(stat) ± 2.8(syst) ± 0.13(lumi)
Observed	4
Signal $M_{\mathrm{TH}} = 3000$ GeV	22.7 ± 1.3(stat)

Table 3: Number of expected background events and number of observed data events in the signal region. The signal expectation for a non-rotating black hole model with parameters $M_{\mathrm{D}} = 630$ GeV, $M_{\mathrm{TH}} = 3$ TeV, and one extra dimension is also shown.

7 Interpretation

Using the observed number of data events and the background expectations, upper limits are set on the cross section (σ) $\times$ the branching ratio to dimuons (BR) $\times$ the acceptance (A) of non Standard Model contribution in the signal region. The profile likelihood method with the $\tilde{q}_\mu$ test statistic [33] is used to derive the upper limits. All statistical and systematic uncertainties on the background are taken into account. The 95% confidence level limit on $\sigma \times BR \times A$ derived from the data in the signal region is 0.148 pb. This limit is stronger than the expected limit of 0.277 pb and falls between the 1σ and 2σ ranges of the expected limit. To avoid the statistical fluctuation that strengthened the result, ATLAS

quotes as the final result of the measurement a limit of 0.184 pb, which is not based on the signal region data but instead lies 1σ below the estimated median sensitivity.

Limits on the reduced Planck mass (M_{D}) and the minimum mass of the black hole (M_{TH}) are set for several models. No theoretical uncertainty on signal prediction is assessed, that is, the exclusion limits are set for the exact benchmark models as implemented in the BlackMax generator. The signal yield is affected by the choice of PDF used for generation. For the signal prediction, two choices of PDFs are considered, CTEQ66 and MRST2007, and the exclusion limits are derived for each of those sets. No PDF uncertainty is included in the limit calculation, rather the difference between CTEQ66 and MRST2007 prediction illustrates the size of the effect. This approach is motivated by the fact that the difference between CTEQ66 and MRST2007 predictions is larger than the uncertainty estimated from the CTEQ66 error set. At the large values of M_{TH} near the quoted limits, the invariant mass of the incoming partons is large and the PDFs are being used in a range of x where they are not well constrained. The signal prediction from MRST2007 is typically 40 to 50% higher than that from CTEQ66 for $M_D = 1$ TeV, $M_{TH} = 3.5$ TeV, while the error on the CTEQ66 prediction is of the order of 3% for these parameters. The difference from the two PDF sets gets larger at higher masses.

The observed results are used to obtain exclusion contours in the plane of M_{D} and M_{TH}. For a large number of points in the $(M_{\mathrm{D}}, M_{\mathrm{TH}})$ plane, the signal acceptance is measured using generator level truth information. This truth-level acceptance is compared to the acceptance from full detector simulation for a smaller set of model points. To account for the difference in acceptances, the truth level acceptance is scaled by a constant factor of 0.85 ± 0.05 which is measured using the set of fully simulated points. The uncertainty is obtained from the RMS of the distribution of difference in acceptance between truth level and fully reconstructed level. Therefore the uncertainty on the signal prediction includes three components: the uncertainty on the scaling factor, on the luminosity of the data sample, and a statistical uncertainty due to the finite MC statistics.

Figure 3 shows the expected and observed exclusion contours for the non-rotating black hole scenario for 2, 4, and 6 extra dimensions. As explained above, ATLAS quotes as the final result a limit that is 1σ stronger than the median sensitivity (the solid line on the plots), instead of the unconstrained limit obtained from data (the dash-dotted line). Figure 4 shows the contours for rotating black holes. In both rotating and non-rotating cases, the contours are shown for the CTEQ66 case and the MRST2007 case. The higher signal prediction in case of MRST2007 leads to a larger exclusion region. The figures also show lines of constant slope ($M_{\mathrm{D}}/M_{\mathrm{TH}}$) of 3, 4 and 5. The semi-classical approximations used for black hole production and decay are only valid for slopes much larger than 1.

In summary, a search for extra dimensions in the same-sign dimuon final state has been performed. No excess over the Standard Model was observed and exclusion contours were obtained in the plane of the reduced Planck scale (M_{D}) and the mass of the black hole (M_{TH}), as well as a model independent limit on any new physics contribution in the signal region was also set.

References

[1] N. Arkani-Hamed, S. Dimopoulos, and G. R. Dvali, *The hierarchy problem and new dimensions at a millimeter*, Phys. Lett. **B429** (1998) 263–272, arXiv:hep-ph/9803315.

[2] I. Antoniadis, N. Arkani-Hamed, S. Dimopoulos, and G. R. Dvali, *New dimensions at a millimeter to a Fermi and superstrings at a TeV*, Phys. Lett. **B436** (1998) 257–263, arXiv:hep-ph/9804398.

[3] N. Arkani-Hamed, S. Dimopoulos, and G. R. Dvali, *Phenomenology, astrophysics and cosmology of theories with sub-millimeter dimensions and TeV scale quantum gravity*, Phys. Rev. **D59** (1999) 086004, arXiv:hep-ph/9807344.

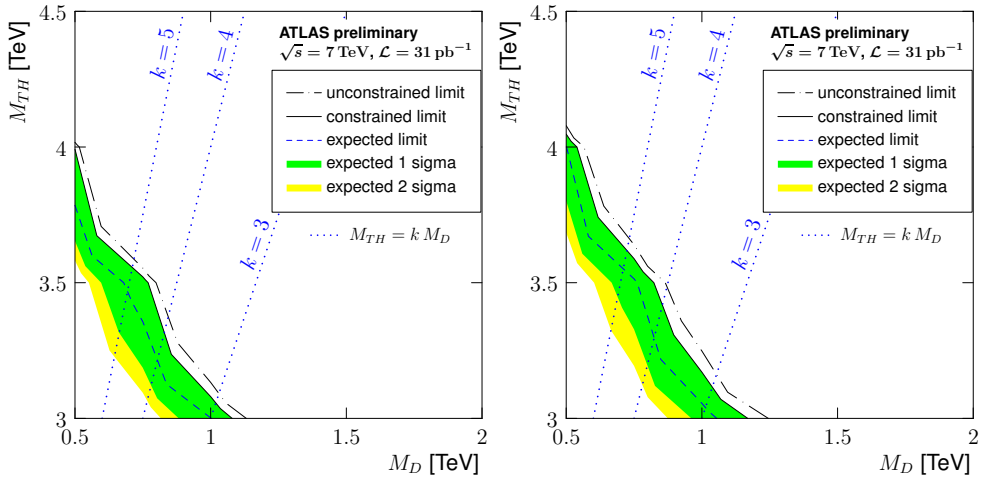

(a) Exclusion contour for non-rotating black holes with 2 extra dimensions

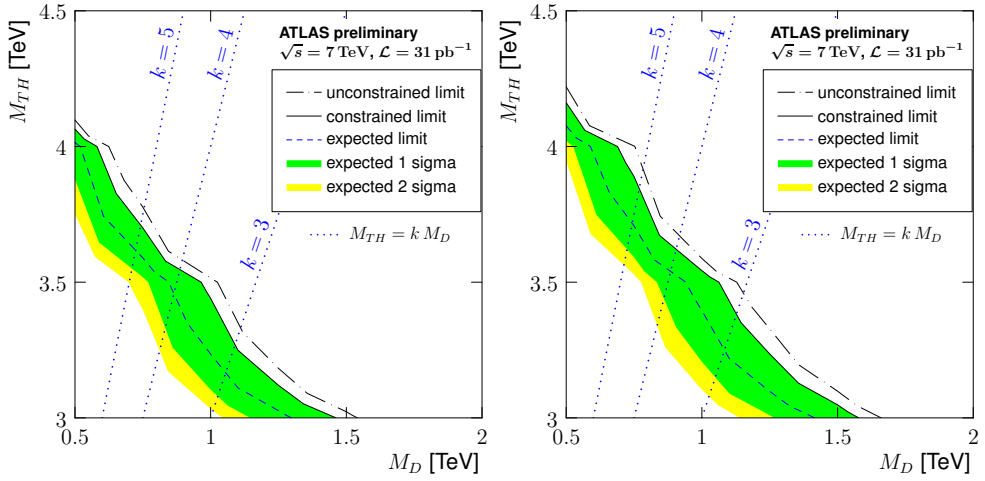

(b) Exclusion contour for non-rotating black holes with 4 extra dimensions

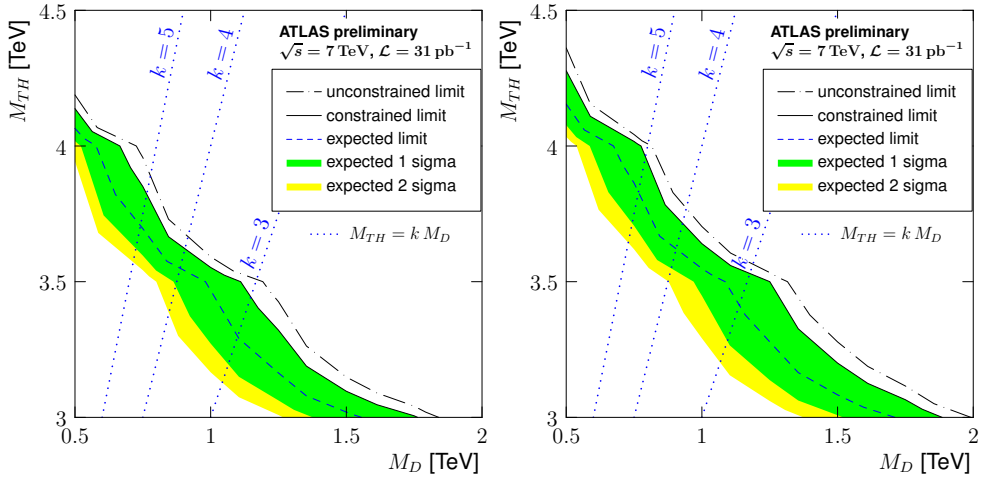

(c) Exclusion contour for non-rotating black holes with 6 extra dimensions

Figure 3: 95% C.L. exclusion contours for non-rotating black holes taking into account all statistical and systematic uncertainties. The top row is for two extra dimensions, the middle for four, and the bottom for six extra dimensions. The left(right) column corresponds to signal generation with the CTEQ66(MRST2007) PDF set. The dashed blue line shows the expected exclusion contour with the 1 and 2 σ uncertainty in green and yellow respectively. The solid black line shows a constrained limit at the 1σ boundary of the estimated sensitivity, which is quoted as the final result. The region below the contour has been excluded by this analysis. The dash-dotted line is the unconstrained limit derived from data. It lies within the 2σ band of the expected limit, however this yellow band is not shown on that side of the sensitivity contour. The figures show lines of constant slope equal to 3,4, and 5. Only slopes much larger than 1 correspond to physical models.

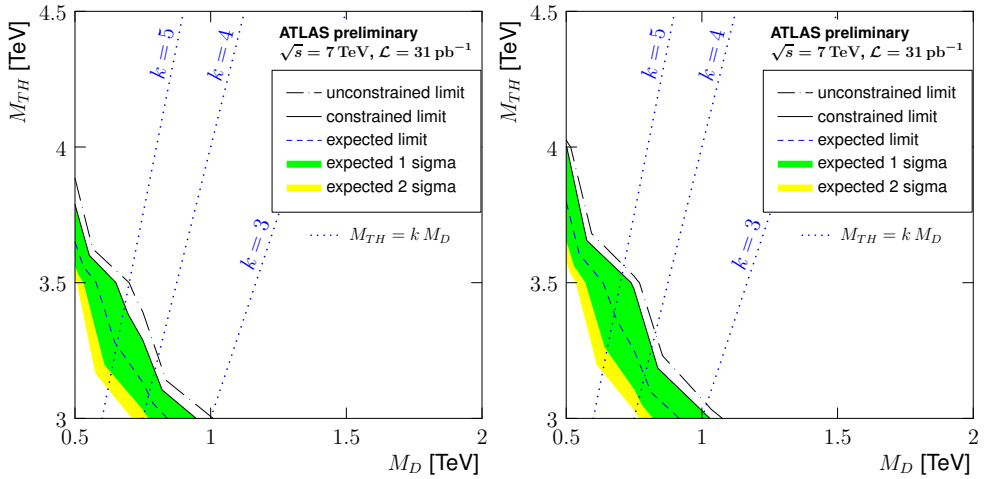

(a) Exclusion contour for rotating black holes with 2 extra dimensions

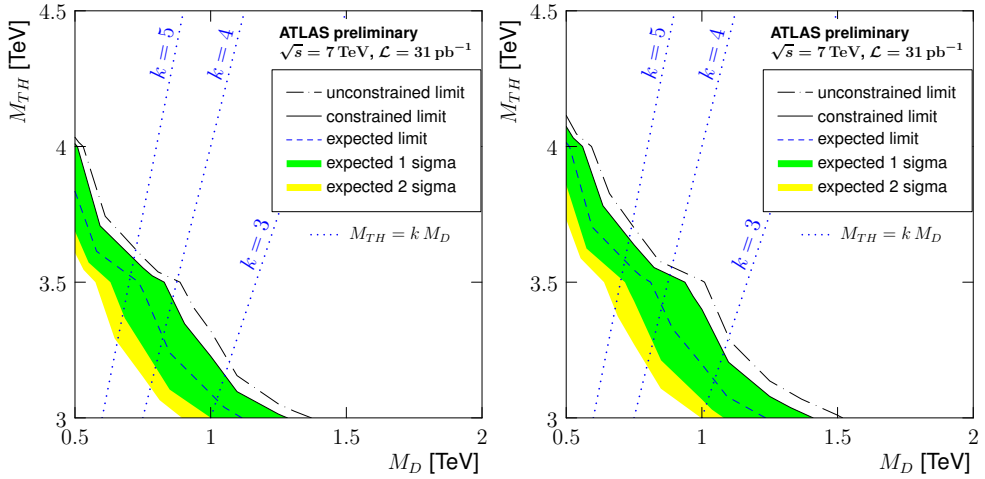

(b) Exclusion contour for rotating black holes with 4 extra dimensions

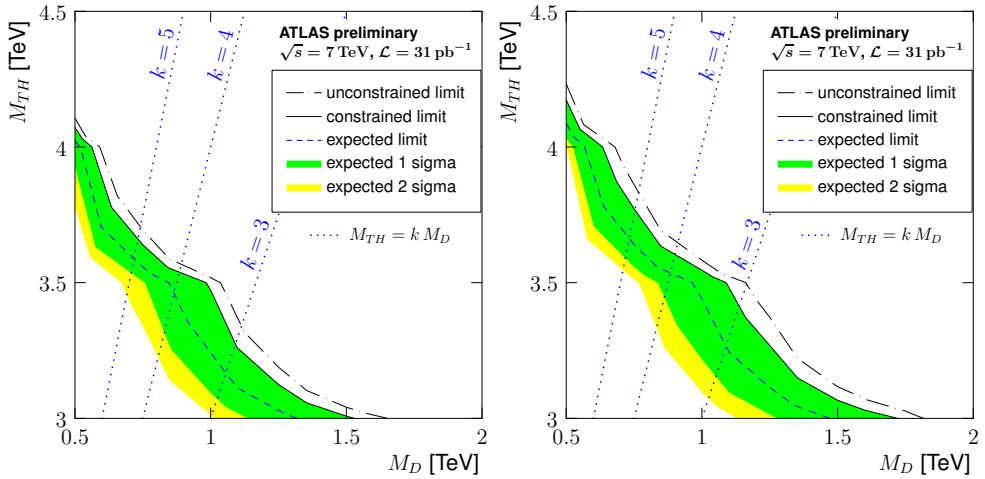

(c) Exclusion contour for rotating black holes with 6 extra dimensions

Figure 4: 95% C.L. exclusion contours for rotating black holes taking into account all statistical and systematic uncertainties. The top row is for two extra dimensions, the middle for four, and the bottom for six extra dimensions. The left(right) column corresponds to signal generation with the CTEQ66(MRST2007) PDF set. The dashed blue line shows the expected exclusion contour with the 1 and 2 σ uncertainty in green and yellow respectively. The solid black line shows a constrained limit at the 1σ boundary of the estimated sensitivity, which is quoted as the final result. The region below the contour has been excluded by this analysis. The dash-dotted line is the unconstrained limit derived from data. It lies within the 2σ band of the expected limit, however this yellow band is not shown on that side of the sensitivity contour. The figures show lines of constant slope equal to 3,4, and 5. Only slopes much larger than 1 correspond to physical models.

[4] LEP Exotica Working Group, ALEPH, DELPHI, L3, and OPAL Collaborations, *Combination of LEP Results on Direct Searches for Large Extra Dimensions*, . CERN Note LEP Exotica WG 2004-03.

[5] CDF Collaboration, T. Aaltonen et al., *Search for large extra dimensions in final states containing one photon or jet and large missing transverse energy produced in $p\bar{p}$ collisions at $\sqrt{s}$ = 1.96-TeV*, Phys. Rev. Lett. **101** (2008) 181602, arXiv:0807.3132 [hep-ex].

[6] D0 Collaboration, V. M. Abazov et al., *Search for large extra dimensions via single photon plus missing energy final states at $\sqrt{s}$ = 1.96-TeV*, Phys. Rev. Lett. **101** (2008) 011601, arXiv:0803.2137 [hep-ex].

[7] K. S. Thorn, *Nonspherical gravitational collapse: A short review*. W.H.Freeman & Co Ltd, San Francisco, 2002. In Magic Without Magic: John Archibald Wheeler.

[8] S. Dimopoulos and G. L. Landsberg, *Black Holes at the LHC*, Phys. Rev. Lett. **87** (2001) 161602, arXiv:hep-ph/0106295.

[9] S. Hawking, *Particle Creation by Black Holes*, Commun.Math.Phys. **43** (1975) 199–220.

[10] D. C. Dai et al., *BlackMax: A black-hole event generator with rotation, recoil, split branes and brane tension*, Phys.Rev. **D77** (2008) 076007, arXiv:0711.3012 [hep-ph].

[11] D. C. Dai et al., *Manual of BlackMax, a black-hole event generator with rotation, recoil, split branes and brane tension*, arXiv:0902.3577 [hep-ph].

[12] ATLAS Collaboration, *Search for new physics in multi-body final states at high invariant masses with ATLAS*, Tech. Rep. ATLAS-CONF-2010-088, CERN, Geneva, Aug, 2010.

[13] CMS Collaboration, V. Khachatryan et al., *Search for Microscopic Black Hole Signatures at the Large Hadron Collider*, Phys. Lett. **B697** (2011) 434–453, arXiv:1012.3375 [hep-ex].

[14] ATLAS Collaboration, *Dimuon composition in ATLAS at 7 TeV*, Tech. Rep. ATL-CONF-2011-003, CERN, Geneva, 2010.

[15] ATLAS Collaboration, G. Aad et al., *The ATLAS Experiment at the CERN Large Hadron Collider*, JINST **3** (2008) S08003.

[16] ATLAS Collaboration, *Updated Luminosity Determination in pp Collisions at $\sqrt{(s)}$ = 7 TeV using the ATLAS Detector*, Tech. Rep. ATL-CONF-2011-011, CERN, Geneva, 2011.

[17] S. Fixione and B. Webber, *Matching NLO QCD computations and parton shower simulations*, JHEP **06** (2002) 029, arXiv:0204244 [hep-ph].

[18] S. Fixione, P. Nason, and B. Webber, *Matching NLO QCD and parton showers in heavy flavour production*, JHEP **08** (2003) 007, arXiv:0305252 [hep-ph].

[19] A. Sherstnev and R. S. Thorne, *Parton Distributions for LO Generators*, arXiv:0711.2473 [hep-ph].

[20] G. Corcella et al., *HERWIG 6.5: an event generator for Hadron Emission Reactions With Interfering Gluons (including supersymmetric processes)*, JHEP **01** (2001) 010, arXiv:0011363 [hep-ph].

[21] J. M. Butterworth et al., *Multiparton interactions in photoproduction at HERA*, Z.Phys.C **72** (1996) 637.

[22] ATLAS Collaboration, *ATLAS Monte Carlo tunes for MC09*, Tech. Rep. ATL-PHYS-PUB-2010-002, CERN, Geneva, Mar, 2010.

[23] P. M. Nadolsky, *Implications of CTEQ global analysis for collider observables*, Phys.Rev. **D78** (2008) 031004, arXiv:0802.0007 [hep-ph].

[24] M. Cacciari, G. P. Salam, and G. Soyez, *The anti-kt clustering algorithm*, JHEP **0804** (2008) 063, arXiv:0802.1189 [hep-ph].

[25] Atlas Collaboration, G. Aad et al., *Measurement of inclusive jet and dijet cross sections in proton-proton collisions at 7 TeV centre-of-mass energy with the ATLAS detector*, Eur. Phys. J. **C71** (2011) 1512, arXiv:1009.5908 [hep-ex].

[26] ATLAS Collaboration, *A measurement of the ATLAS muon reconstruction and trigger efficiency using J/psi decays*, Tech. Rep. ATLAS-CONF-2011-021, CERN, Geneva, Jan, 2011.

[27] ATLAS Collaboration, *Determination of the muon reconstruction efficiency in ATLAS at the Z resonance in proton-proton collisions at* $\sqrt{(s)} = 7$ TeV, Tech. Rep. ATLAS-CONF-2011-008, CERN, Geneva, Feb, 2011.

[28] ATLAS Collaboration, G. Aad et al., *Charged-particle multiplicities in pp interactions measured with the ATLAS detector at the LHC*, arXiv:1012.5104 [hep-ex].

[29] M. Aliev et al., *HATHOR HAdronic Top and Heavy quarks crOss section calculatoR*, arXiv:1007.1327 [hep-ph].

[30] Atlas Collaboration, G. Aad et al., *Measurement of the top quark-pair production cross section with ATLAS in pp collisions at* $\sqrt{s} = 7$ TeV, arXiv:1012.1792 [hep-ex].

[31] P. Nason, *A new method for combining NLO QCD with shower Monte Carlo algorithms*, JHEP **11546** (2004) 040.

[32] B. P. Kersevan and E. Richter-Was, *The Monte Carlo event generator AcerMC version 2.0 with interfaces to PYTHIA 6.2 and HERWIG 6.5*, arXiv:0405247 [hep-ph].

[33] G. Cowan, K. Cranmer, E. Gross, and O. Vitells, *Asymptotic formulae for likelihood-based tests of new physics*, Eur.Phys.J. **C71** (2011) 1554, arXiv:1007.1727 [physics.data-an].

8 Extra Plots

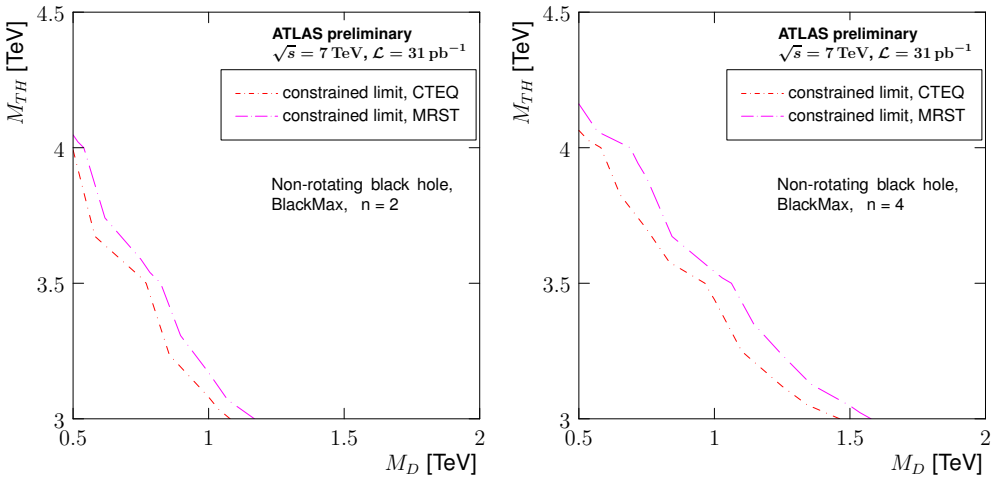

(a) Exclusion contour for non rotating black holes with 2 extra dimensions

(b) Exclusion contour for non rotating black holes with 4 extra dimensions

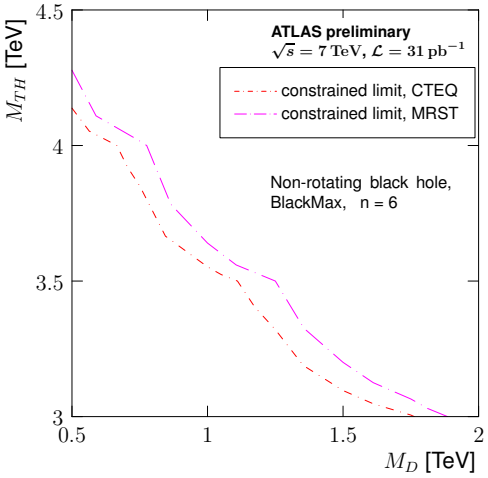

(c) Exclusion contour for non rotating black holes with 6 extra dimensions

Figure 5: 95% confidence level exclusion contours for non rotating black holes taking into account all statistical and systematic uncertainties. Figures 5(a), 5(b), and 5(c) show the contours for two, four and six extra dimensions respectively. The constrained limits are shown for signal generated with CTEQ66 and with MRST2007 PDF sets.

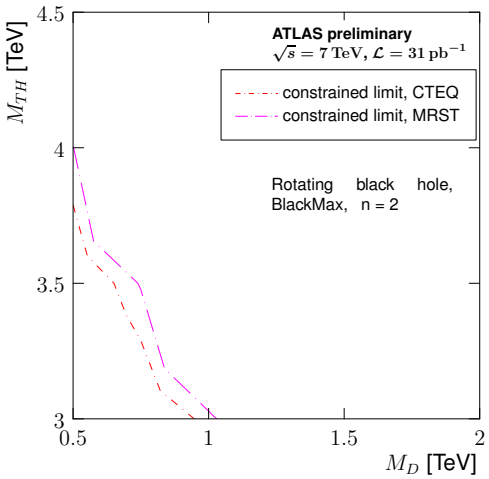

(a) Exclusion contour for rotating black holes with 2 extra dimensions

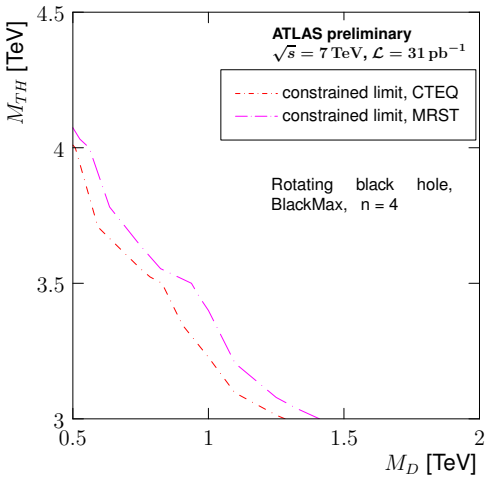

(b) Exclusion contour for rotating black holes with 4 extra dimensions

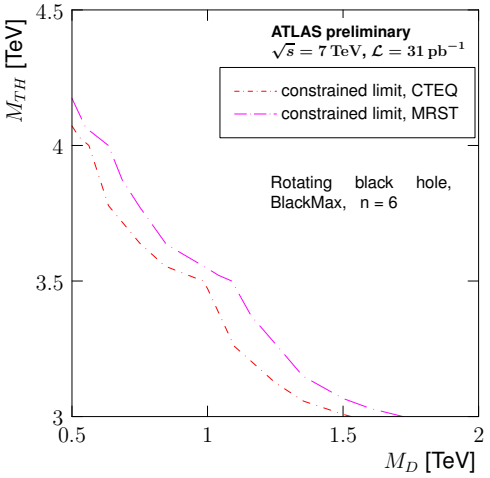

(c) Exclusion contour for rotating black holes with 6 extra dimensions

Figure 6: 95% confidence level exclusion contours for rotating black holes taking into account all statistical and systematic uncertainties. Figures 6(a), 6(b), and 6(c) show the contours for two, four and six extra dimensions respectively. The constrained limits are shown for signal generated with CTEQ66 and with MRST2007 PDF sets.